Intermetallics 46 (2014) 211–221

Contents lists available at ScienceDirect

Intermetallics

journal homepage: www.elsevier.com/locate/intermet

First-principle calculations of structural, elastic and thermodynamic properties of Fe–B compounds

Liu-Hui Li, Wei-Li Wang, Liang Hu, Bing-Bo Wei*

MOE Key Laboratory of Space Applied Physics and Chemistry, Northwestern Polytechnical University, Xi'an 710072, China

ARTICLE INFO

Article history:
Received 18 July 2013
Received in revised form
6 November 2013
Accepted 11 November 2013
Available online 10 December 2013

Keywords:
A. Intermetallics, miscellaneous
B. Elastic properties
B. Thermodynamic and thermochemical properties
E. Ab-initio calculations

ABSTRACT

The structural, elastic and thermodynamic properties of FeB, Fe_2B, orthorhombic and tetrahedral Fe_3B, FeB_2 and FeB_4 iron borides are investigated by first-principle calculations. The elastic constants and polycrystalline elastic moduli of Fe–B compounds are usually large especially for FeB_2 and FeB_4, whose maximum elastic constant exceeds 700 GPa. All of the six compounds are mechanically stable. The Vickers hardness of FeB_2 is estimated to be 31.4 GPa. Fe_2B and FeB_2 are almost isotropic, while the other four compounds have certain degree of anisotropy. Thermodynamic properties of Fe–B compounds can be accurately predicted through quasi-harmonic approximation by taking the vibrational and electronic contributions into account. Orthorhombic Fe_3B is more stable than tetrahedral one and the phase transition pressure is estimated to be 8.3 GPa.

1. Introduction

The binary Fe–B alloy system has been subjected to many experimental and theoretical studies in the past decades [1–10]. It attracts so much attention due to not only the interesting metastable phase formation during rapid solidification, but also its special mechanical and magnetic properties. So far, FeB, Fe_2B, orthorhombic Fe_3B (*o*-Fe_3B), tetragonal Fe_3B (*t*-Fe_3B), FeB_2 and FeB_4 iron borides have been reported and investigated to different extents. According to the equilibrium Fe–B phase diagram, there are two stable iron borides, FeB and Fe_2B at ambient temperature [8]. The metastable *o*-Fe_3B and *t*-Fe_3B have also been obtained by quenching and annealing from Fe–B glasses [7,8]. Recently, two novel Fe–B compounds have been found to show special properties: *oP*12-FeB_2 is expected to be the first semiconducting metal diboride and *oP*10-FeB_4 may display phonon-mediated superconductivity with a critical temperature T_c of 15–20 K [4].

The electronic and magnetic properties of the Fe–B compounds have been investigated in detail [1–4]. However, the equations of state (EOS's) for these compounds have not been presented. They are able to provide much information of the equilibrium properties and even the high temperature thermodynamic properties [11–13]. The understanding of the special mechanical properties of Fe–B compounds needs the knowledge of their elastic constants and polycrystalline bulk moduli. Although the elastic moduli of some Fe–B compounds have been reported, there are not enough detailed analyses [5,10]. Thermodynamic properties of materials are of great importance in many aspects. For the stable FeB and Fe_2B phases, a number of thermodynamic data have been generated including the enthalpy of formation, Gibbs free energy of formation, partial enthalpy of mixing and activity of B [9]. Based on these data, thermodynamic modeling of Fe–B system was assessed by calculation of phase diagram (CALPHAD) approach [9]. To get further insight into the detailed structural, mechanical and thermodynamic properties of Fe–B system especially for the new FeB_2, FeB_4 and two metastable Fe_3B phases, a systematic investigation is necessary.

Due to the advantage of requiring only atomic species and crystal structures, first-principle calculations have been widely used to study the structural and elastic properties of various substances [1,3,14,15]. Recently, first-principle calculations together with quasi-harmonic approximation are used to predict the thermodynamic properties of solids at high temperatures [11–13,16–19]. These approaches can provide reliable prediction of thermodynamic properties when experimental information is lacking or in controversy, and are therefore employed in this work.

The present work aims to predict the structural, elastic and thermodynamic properties of Fe–B compounds in the light of first-principles phonon and Debye approach. In this paper, we firstly present the theory and methodology of first-principle calculations,

* Corresponding author.
E-mail address: bbwei@nwpu.edu.cn (B.-B. Wei).

0966-9795/$ – see front matter © 2013 Elsevier Ltd. All rights reserved.
http://dx.doi.org/10.1016/j.intermet.2013.11.007

the phonon model and Debye model to predict thermodynamic properties. Next, we present and discuss the main results in comparison with results from other experiments or theoretical calculations. Finally, a summary of this work is derived.

2. Computational methods

2.1. 0K Properties and phonon calculations

The first-principle calculations of all the mentioned Fe–B compounds have been performed by density functional theory (DFT). The generalized gradient approximation (GGA) approach [20] in the form of Perdew–Burke–Ernzerhof (PBE) [21] is adopted. The projector augmented wave (PAW) pseudopotential [22], as implemented in the Vienna *ab initio* Simulation Package (VASP) [23,24], is used to describe the electron–core interactions. The electron configurations are $3p^6 3d^7 4s^1$ and $2s^2 2p^1$ for Fe and B atoms, respectively. In VASP calculations, the energy convergence criterion for electronic self-consistency is 1×10^{-6} eV/cell. The energy cutoff is chosen as 500 eV which is large enough to make the energy error less than 1×10^{-4} eV/cell. The wave functions are sampled on Monkhorst–Pack [25] *k*-meshes and optimized before any further calculations. In the structure optimization processes, all the degrees of freedom are allowed to relax. The reciprocal space energy integrations are carried out by the Methfessel–Paxton smearing method [26] with an appropriate energy width. After relaxations, a final static energy calculation is performed with the tetrahedron method by Blöchl correction [27]. During all the calculations, the spin-polarized approximation is adopted due to the ferromagnetic nature of Fe-contained materials.

In order to describe the equilibrium structural properties and thermodynamic properties from first-principles, the energy–volume relationships of the compounds are calculated at different volumes and fitted by 4-order Birch–Murnaghan (BM) equation of state (EOS). During the fitting, the method of strain polynomials is adopted owing to the possibility of linear fitting together with the advantage of numerical stability [17,18]. The strain polynomials of BM EOS employed here have the following general form [17]:

$$E(f) = \sum_{k=0}^{n} c_k f^k \tag{1}$$

where $f = 1/2^*(x^{-2} - 1)$ and $x = (V/V_0)^{1/3}$, c_k are the fitting parameters. When $n = 4$, it is the 4-order EOS used in the present work. The equilibrium properties, i.e., the volume V_0, energy E_0, bulk modulus B_0 and its pressure derivatives B_0' can be derived from the fitted EOS [18].

The phonon properties of Fe–B compounds are calculated by PHONOPY [28,29] with VASP the calculation engine. The Hellman–Feynman forces on the atoms are calculated through density functional perturbation theory (DFPT) [30]. The force constants can be obtained based on the calculated forces [29]. The phonon dispersions and phonon density of states (PhDOS) of Fe–B compounds can be then derived by PHONOPY and used for thermodynamic calculations.

2.2. Elastic constants

The strain energy versus strain method is adopted to calculate the elastic constants. The internal energy E of a crystal under a general strain δ_{ij} can be expressed by expanding E of the deformed crystal with respect to the strain tensor in terms of Taylor's series [14]:

$$E(V) = E(V_0, 0) + V_0 \sum_{ij} \sigma_{ij}\delta_{ij} + \frac{V_0}{2} \sum_{ijkl} c_{ijkl}\delta_{ij}\delta_{kl} + \cdots \tag{2}$$

where σ_{ij} is the stress tensor element, V_0 and E_0 are the volume and energy of the undeformed crystal, respectively. The subscripts of strain tensor (ij, kl) can be expressed in Voigt notation scheme ($11 = 1, 22 = 2, 33 = 3, 23 = 4, 31 = 5, 12 = 6$). c_{ijkl} is the element of elastic constant tensor, it can be derived from the second-order coefficient of a polynomial fit to the strain energy with respect to the strain.

The original crystal structure R will be distorted to structure R' after applying a small deformation, which gives $R' = RD$, where D is the deformation matrix. For a given set of strains $s = (s_1, s_2, s_3, s_4, s_5, s_6)$, the deformation matrix is defined by [14]:

$$D = \begin{bmatrix} s_1 & s_6/2 & s_5/2 \\ s_6/2 & s_2 & s_4/2 \\ s_5/2 & s_4/2 & s_3 \end{bmatrix} \tag{3}$$

Six strains are applied to each deformation matrix, where the strain values are ±0.005, ±0.01 and ±0.02 times of the corresponding lattice constants. According to the numbers of independent elastic constants for different crystals, the number of deformation matrices applied to cubic, hexagonal, tetragonal, orthogonal and monoclinic structures are 3, 5, 6, 9 and 13, respectively [14].

2.3. Thermodynamic properties

The Gibbs free energy G of a given structure at volume V and temperature T can be represented by:

$$G(V, T) = E_c(V) + F_{vib}(V, T) + F_{el}(V, T) + pV \tag{4}$$

where p is the applied external pressure, $E_c(V)$ is the static energy at 0 K which can be obtained directly from first-principle calculations, $F_{vib}(V, T)$ and $F_{el}(V, T)$ are the lattice vibrational contribution and thermal electronic contribution (TEC) to Gibbs free energy, respectively.

The vibrational free energy can be well described by the quasi-harmonic approximation (QHA) which takes the volume expansion effect into account. Based on QHA method, the Debye or phonon model can be used to calculate various thermodynamic properties [11–13]. In the phonon model, from the phonon density of states, the vibrational free energy can be calculated by [11]:

$$F_{vib}(T) = k_B T \int_0^\infty \ln\left[2 \sin h\left(\frac{\hbar\omega}{2k_B T}\right)\right] g(\omega) \mathrm{d}\omega \tag{5}$$

where k_B is Boltzmann's constant,$\hbar$ is the reduced Planck's constant, $g(\omega)$ is the phonon density of states. Based on phonon DOS, the nth moment Debye cutoff frequency and the corresponding nth moment Debye temperature can be determined [12]. The nth moment Debye temperature Θ_D can be obtained by:

$$\Theta_D(n) = \hbar\omega_n / k_B \tag{6}$$

In a Debye solid, different values of n correspond to different thermodynamic properties, e.g., $\Theta_D(2)$ is usually related to the Debye temperature obtained from the specific heat [12] and is used in this work. The phonon properties for each structure are calculated at eight volumes around the equilibrium one.

In the Debye model, F_{vib} is calculated as a function of Debye temperature Θ_D:

$$F_{\mathrm{vib}}(V,T) = \frac{9}{8}k_{\mathrm{B}}\Theta_{\mathrm{D}} + k_{\mathrm{B}}\left\{3\ln\left[1 - \exp\left(-\frac{\Theta_{\mathrm{D}}}{T}\right)\right] - D\left(\frac{\Theta_{\mathrm{D}}}{T}\right)\right\} \quad (7)$$

where $D(x) = 3/x^3\int_0^x t^3/[\exp(t)-1]\mathrm{d}t$ is the Debye function. In Debye model, Θ_{D} is calculated by [17]:

$$\Theta_{\mathrm{D}} = \frac{1}{k_B}\left(6\pi^2 V^{1/2} n\right)^{1/3} f(\sigma)\sqrt{\frac{B_{\mathrm{sta}}}{M}} \quad (8)$$

where V and M are the volume and molecular mass per cell, respectively. B_{sta} and σ are the static bulk modulus and Poisson's ratio at the equilibrium structure, $f(\sigma)$ is a function of σ. The approximate Grüneisen ratio γ_D has the form of [17]:

$$\gamma_D = a + b\frac{\mathrm{d}\,B_{\mathrm{sta}}}{\mathrm{d}\,p} = a - b\frac{\mathrm{d}\ln B_{\mathrm{sta}}}{\mathrm{d}\ln p} \quad (9)$$

This is the general expression consistent with some approximation including the expression of Slater ($a = -1/6$ and $b = 1/2$), Dugdale–McDonald ($a = -1/2$ and $b = 1/2$) and Vaschenko–Zubarev ($a = -5/6$ and $b = 1/2$) [17].

Thermal electronic contribution is not negligible especially in the case of metals, its contribution to Gibbs free energy is given by [31]:

$$E_{\mathrm{el}}(V,T) = \int n(\varepsilon)f\varepsilon\mathrm{d}\varepsilon - \int^{\varepsilon_{\mathrm{F}}} n(\varepsilon)\varepsilon\mathrm{d}\varepsilon \quad (10)$$

where $n(\varepsilon)$ is the electronic DOS, f is the Fermi function and the electron chemical potential should be calculated self-consistently. The electronic entropy can be calculated by [31]:

$$S_{\mathrm{el}}(V,T) = -k_{\mathrm{B}}\int n(\varepsilon,V)[f\ln f + (1-f)\ln(1-f)]\mathrm{d}\varepsilon \quad (11)$$

The electronic free energy can be then expressed by:

$$F_{\mathrm{el}}(V,T) = E_{\mathrm{el}}(V,T) - TS_{\mathrm{el}}(V,T) \quad (12)$$

With the above equations, the Gibbs free energy at any given temperature can be minimized with respect to the volume. The other thermodynamic properties can be obtained according to thermodynamic relationships [17].

3. Results and discussions

3.1. Equilibrium structural properties

The structures and optimized lattice parameters together with other cited results for α-Fe, α-B and Fe–B compounds are presented in Table 1. The deviations are also presented. It is evident that the calculated results in this work are in good agreement with other data especially for FeB_2 and FeB_4. The maximum deviation is 1.65% for FeB.

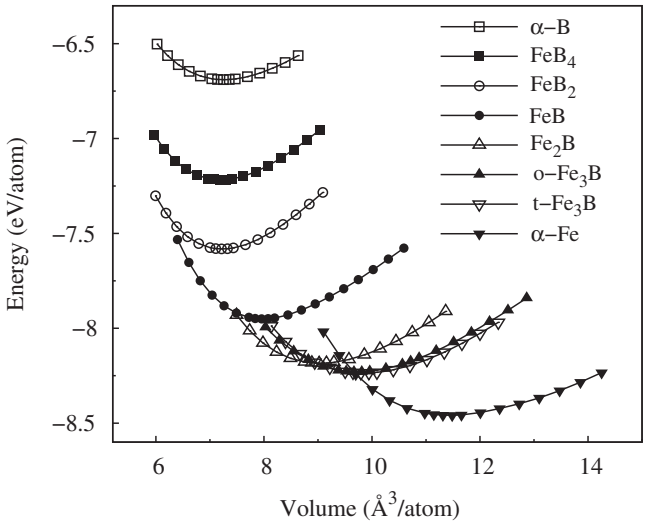

Fig. 1. Energy–volume relationships of Fe–B system.

The energy–volume relationships which can provide valuable equilibrium information of these compounds are shown in Fig. 1. From the cold energy–volume curve and the 4-order Birch–Murnaghan equation of state, the equilibrium structural properties including the equilibrium volume V_0, energy E_0, bulk modulus B_0 and its pressure derivatives B_0', and the average magnetic moments per Fe atom μ_{Fe} are derived as shown in Table 2, other available experimental or calculated results are also presented for comparison. In general, the average atomic volumes of these iron borides increase with Fe atom content since Fe atom is obviously larger than B atom. However, it is interesting to mention that the average atomic volumes of FeB_2 and FeB_4 are smaller than that of α-B, which indicating the denser atom arrangement of these two compounds than α-B. The deviations of the volumes from this work and other results are usually less than 4%.

From Table 2, the bulk moduli (B_0) of α-Fe and α-B agree well with other experimental results. The bulk moduli of all the six iron borides are larger than that of α-Fe, although for both *o*- and *t*-Fe_3B they are a little smaller than that of α-B, which suggests the possible high hardness of Fe–B compounds. The pressure derivatives of bulk modulus B_0's are around the value of 4.0 except for α-Fe. For both two Fe_3B structures, B_0's are about 3.35 as the lowest among the six Fe–B compounds. For the average magnetic moment per Fe atom μ_{Fe} (in unit of Bohr magneton μ_{B}), it is found that this work gives quite satisfactory results for Fe–B system. The largest discrepancy rests in *o*-Fe_3B. The boron-rich compounds FeB_2 and FeB_4 are not spin polarized according to the zero magnetic moments.

Table 1
Crystal structures and lattice parameters of Fe–B system.

Substances	Pearson symbol	Space group	*a* (Å) This work, Ref. [32]	*b* (Å) This work, Ref. [32]	*c* (Å) This work, Ref. [32]	Maximum error (%)
α-Fe	*cI*2	*Im-3m*	2.835, 2.866			1.08
o-Fe_3B	*oP*16	*Pnma*	5.393, 5.397	6.656, 6.648	4.380, 4.368	0.27
t-Fe_3B	*tI*32	*I-4*	8.551, 8.655		4.240, 4.297	1.20
Fe_2B	*tI*12	*I4/mcm*	5.056, 5.106		4.232, 4.251	0.98
FeB	*oP*8	*Pnma*	5.413, 5.504	2.948, 2.945	3.998, 4.056	1.65
FeB_2	*oP*12	*Pnma*	4.816, 4.819	4.807, 4.807	3.740, 3.742	0.06
FeB_4	*oP*10	*Pnnm*	4.521, 4.526	5.284, 5.284	3.006, 3.006	0.11
α-B	*hR*36	*R-3mh*	4.901, 4.909		12.556, 12.572	0.13

Table 2
Equilibrium properties of Fe–B system derived from EOS fitting of the energy–volume curves, including the equilibrium volume, cohesive energy, formation energy, bulk modulus and its pressure derivative, average magnetic moment per Fe atom.

Substances	V_0 (Å^3/atom)	E_c (eV)	E_f (eV)	B_0 (GPa)	B'_0	μ_{Fe} (μ_B)
α-Fe	11.39, 11.77[a]	5.061, 4.28[c]		173.6, 168.3[c]	5.35, 4.70[f]	2.22, 2.22[f]
o-Fe_3B	9.85, 9.80[a]	5.689, 6.038[d]	−0.222	191.0	3.34	2.08, 1.95[d]
t-Fe_3B	9.71, 10.06[a]	5.683, 5.644[d]	−0.216, −0.22[b]	204.7	3.36	2.02, 1.99[d]
Fe_2B	9.04, 9.24[a]	5.920	−0.317, −0.31[b]	224.3	4.16	1.90, 1.95[g]
FeB	7.96, 8.26[a]	6.249	−0.376, −0.37[b]	287.5	4.35	1.25, 1.26[g]
FeB_2	7.22, 7.22[b]	6.446	−0.302, −0.30[b]	307.8	4.38	0.00, 0.00[b]
FeB_4	7.19, 7.18[b]	6.532	−0.172, −0.17[b]	266.9	4.04	0.00, 0.00[b]
α-B	7.25, 7.28[a]	6.686, 5.81[c]		211.2, 238.4[e]	3.94	0.00

[a] Ref. [32].
[b] Ref. [4].
[c] Ref. [33].
[d] Ref. [3].
[e] Ref. [34].
[f] Ref. [35].
[g] Ref. [1].

The enthalpy of formation (E_f) and cohesive energy (E_c) of the compounds are calculated by:

$$E_f(Fe_xB_y) = \frac{1}{x+y}\left[E(Fe_xB_y) - xE_b(Fe) - yE_b(B)\right] \quad (13)$$

$$E_c(Fe_xB_y) = -\frac{1}{x+y}\left[E(Fe_xB_y) - xE_a(Fe) - yE_a(B)\right] \quad (14)$$

where $E(Fe_xB_y)$ is the energy of Fe_xB_y compounds, E_a(Fe) and E_a(B) are the energy of isolated Fe or B atom, E_b(Fe) and E_b(B) are the energy of bulk Fe and B, respectively. The energies for bulk materials are derived from the EOS fitting of the energy–volume curves. It is noteworthy that for bulk materials, the ground state of Fe is selected as α-Fe, whereas for B this is selected as α-B which is found to be a little higher in energy than β-B but has a much simpler structure [36].

The calculated energies are presented in Table 2. The formation energy of all the compounds coincides very well with other theoretical results [4]. The cohesive energy of o-Fe_3B is E_c = 5.689 eV/atom = 548.9 kJ/mol which is a little lower than the value of 582 kJ/mol from LMTO calculation [3], while for t-Fe_3B E_c = 5.683 eV/atom = 548.2 kJ/mol which is very close to the LMTO value of 544 kJ/mol. However, the difference between the cohesive energy of both o- and t-Fe_3B in this work is very small (about 0.7 kJ/mol), while from LMTO calculation this is 38 kJ/mol, the deviation maybe rely on the calculation method, the selection of calculation parameters and so on. It is well known that the lower the energy, the more stable the structure is. From Fig. 1 and the calculated cohesive energies, we can conclude that o-Fe_3B has lower energy than t-Fe_3B and is thus more stable.

3.2. Elastic properties

The elastic constants of single crystalline Fe–B compounds are presented in Table 3. Generally, the elastic constants along three principle axes (a-, b- and c-) are very high especially for FeB_2 and FeB_4, which indicates the high resistance to linear compression in these directions. However, the magnitude orders in three axes are different. For orthorhombic FeB and Fe_3B, the order is $c_{33} > c_{22} > c_{11}$. In the case of orthorhombic FeB_2 and FeB_4, c_{22} is larger than c_{11} and c_{33} and exceeds 700 GPa, suggesting the extremely large stiffness for these two compounds along b axis. For tetragonal Fe_2B and Fe_3B, c_{33} is smaller than c_{11} and c_{22}.

Since the tetragonal structure can be regarded as the special situation of orthorhombic structure with an additional condition of $a = b$, the mechanical stability criteria for the six iron borides can be represented in a uniform manner for orthorhombic structure [15]:

$$\begin{aligned} &c_{ii} > 0 (i = 1, 2, 3, 4, 5, 6) \\ &c_{11} + c_{22} + c_{33} + 2(c_{12} + c_{13} + c_{23}) > 0 \\ &c_{11} + c_{22} - 2c_{12} > 0, \quad c_{11} + c_{33} - 2c_{13} > 0 \\ &c_{22} + c_{33} - 2c_{23} > 0 \end{aligned} \quad (15)$$

The mechanical stability of all the six iron borides are examined according to the above formula, it is found that all of them are mechanically stable.

The theoretical polycrystalline elastic moduli for Fe–B compounds can be determined from the independent elastic constants. There are two models to evaluate the moduli: the Voigt (V) method and Reuss (R) method, which provide the upper and lower bounds of the polycrystalline elastic modulus, respectively. For different crystalline systems, the shear modulus (G) and bulk modulus (B) according to Voigt can be expressed as [37]:

$$9B_V = (c_{11} + c_{22} + c_{33}) + 2(c_{12} + c_{13} + c_{23}) \quad (16)$$

$$15G_V = (c_{11} + c_{22} + c_{33}) - (c_{12} + c_{13} + c_{23}) + 3(c_{44} + c_{55} + c_{66}) \quad (17)$$

and by Reuss that:

$$1/B_R = (s_{11} + s_{22} + s_{33}) + 2(s_{12} + s_{13} + s_{23}) \quad (18)$$

$$1/G_R = 4[(s_{11} + s_{22} + s_{33}) - (s_{12} + s_{13} + s_{23})]/15 + (s_{11} + s_{22} + s_{33})/5 \quad (19)$$

where c_{ij}'s are the elements of elastic coefficient matrix and s_{ij}'s are the elements of elastic compliance matrix. The arithmetic average of the Voigt and Reuss bounds is known as the Voigt–Reuss–Hill (VRH) average, which is regarded as the best estimate for the theoretical value of polycrystalline elastic modulus [37]:

$$G_H = (G_R + G_V)/2 \quad (20)$$

$$B_H = (B_R + B_V)/2 \quad (21)$$

The Young's modulus and Poisson's ratio can be computed based on the above values by [37]:

Table 3
Single crystalline elastic constants (in GPa) of Fe–B system.

Substances	c_{11}	c_{22}	c_{33}	c_{44}	c_{55}	c_{66}	c_{12}	c_{13}	c_{23}
α-Fe	266.4			96.3			146.5		
	279.2[a]			93.0[a]			148.8[a]		
	237[b]			116[b]			141[b]		
o-Fe_3B	263.3	302.7	318.4	110.2	101.2	158.7	133.5	162.8	178.6
t-Fe_3B	284.1		278.8	107.2		136.0	167.8	98.5	
Fe_2B	410.3		386.6	147.7		156.9	154.4	122.0	
	413[c]		389[c]	148[c]		157[c]	154[c]	132[c]	
	389.8[d]		282.2[d]	114.0[d]		89.2[d]	169.6[d]	218.5[d]	
FeB	373.7	434.1	503.4	207.4	117.6	193.7	246.0	184.4	209.1
	371[c]	431[c]	505[c]	207[c]	118[c]	194[c]	250[c]	188[c]	209[c]
FeB_2	589.9	719.0	569.5	272.6	201.7	221.8	179.3	153.5	131.4
FeB_4	411.0	760.7	456.1	217.7	140.2	227.7	161.3	152.8	147.4
α-B	453.5		609.5	215.9		180.0	93.5	118.7	
	602.7[e]		596.4[e]	267.4[e]		274.2[e]	54.3[e]	59.0[e]	

[a] Ref. [38].
[b] Ref. [37].
[c] Ref. [5].
[d] Ref. [10].
[e] Ref. [34].

$$E = 9BG/(3B+G) \tag{22}$$

$$\nu = (3B-2G)/(6B+2G) \tag{23}$$

The isotropic elastic moduli of Fe–B compounds are calculated by these equations and presented in Table 4 together with other theoretical results. The bulk modulus can be obtained through either VRH calculation from the elastic constants (B_H) as shown in Table 4 or fitting of EOS (B_0) as shown in Table 2. These two methods often give quite close values.

The bulk modulus B_H, shear modulus G_H and Young's modulus E with respect to B atom content are plotted in Fig. 2. Generally, the three moduli first increase and then decrease with B atom content, the maximum values locate at 66.7 at% B for FeB_2.

The ratio of B/G (here B_H and G_H are used) can be used to estimate the ductility or brittleness of materials, since a high (low) value is associated with ductility (brittleness), and the critical value is about 1.75. Meanwhile, the Poisson's ratio larger or smaller than 0.25 can be also used to represent the ductility or brittleness of materials. The calculated values for Fe–B compounds are presented in Table 4. It is found that FeB and both o- and t-Fe_3B can be classified as ductile since B_H/G_H is larger than 1.75 and ν is larger than 0.25, while Fe_2B, FeB_2 and FeB_4 should be classified as brittle.

The hardness of a material is related to the elastic and plastic properties, there have been some semi-empirical models developed to predict the hardness of materials [39–42]. Recently, Chen et al. proposed a model to predict the hardness of polycrystalline materials and bulk metallic glasses based on the Pugh's modulus ratio ($k = G/B$) and the shear modulus (G) as follows [42]:

$$H_v = 2\left(k^2G\right)^{0.585} - 3 \tag{24}$$

where H_v denotes the Vickers hardness. The results for Fe–B compounds are presented in Table 4. The hardness for Fe_2B is 19.0 GPa, which is in good agreement with the result derived from bond population analysis [10]. The hardness for o-Fe_3B is 9.1 GPa as the smallest one among all the compounds, while for t-Fe_3B it is 12.0 GPa, a little larger than that for o-Fe_3B. The largest value is 31.4 GPa for FeB_2, which is close to the values for β-SiC (32.0–35.5 GPa), ReB_2 (32.9 GPa) and WC (29.3–33.4 GPa) [42], indicating the high hardness of FeB_2.

In order to describe the degrees of anisotropy of Fe–B compounds, the shear anisotropic factors are adopted [14]:

$$A_1 = \frac{4c_{44}}{c_{11}+c_{33}-2c_{13}} \quad \text{for (100) plane} \tag{25}$$

$$A_2 = \frac{4c_{55}}{c_{22}+c_{33}-2c_{23}} \quad \text{for (010) plane} \tag{26}$$

$$A_3 = \frac{4c_{66}}{c_{11}+c_{22}-2c_{12}} \quad \text{for (001) plane} \tag{27}$$

A value of unity indicates isotropy for a crystal while a non-unity value indicates anisotropy. The calculated results are presented in Table 5. It can be seen that Fe_2B has the highest isotropy among all the iron borides since the values are 1.07 for (100) and (010) plane and 1.23 for (001) plane. Both FeB_2 and FeB_4 exhibit low anisotropy. For FeB and two Fe_3B structures, the anisotropy is very strong especially in (001) plane.

The percentages of anisotropy in the compression and shear are another way of measuring the elastic anisotropy as defined by [14]:

$$A_B = \frac{B_V - B_R}{B_V + B_R} \times 100 \tag{28}$$

$$A_G = \frac{G_V - G_R}{G_V + G_R} \times 100 \tag{29}$$

A universal elastic anisotropy index (A^U) which accounts for both the shear and bulk contributions was proposed as [43]:

$$A^U = 5\frac{G_V}{G_R} + \frac{B_V}{B_R} - 6 \geq 0 \tag{30}$$

A^U is identically zero for locally isotropic single crystals. The departure of A^U from zero defines the extent of single crystal anisotropy. The calculated A_B, A_G and A^U are presented in Table 5. The A_B value for α-Fe is identically zero because B_V and B_R are equal; the values for other substances are scattered and not compatible with the trends of A_G and A^U. It is supposed that the factor A_B is insufficient for identify the anisotropy. The A_G value for α-B is 23.9 and is the largest one among all the substances, which indicates the high anisotropy of α-B. This is confirmed by the A^U value of 3.17. Fe_2B and FeB_2 are almost isotropic concluded from all the

Table 4
Polycrystalline elastic properties of Fe–B system, including Bulk modulus (B), shear modulus (G), Young's modulus (E), Poisson's ratio (ν) and Vickers hardness (H_v).

Substances	B_V (GPa)	B_R (GPa)	B_H (GPa)	G_V (GPa)	G_R (GPa)	G_H (GPa)	E_H (GPa)	B_H/G_H	ν	H_v (GPa)
α-Fe	186.5	186.5	186.5	81.7	77.5	79.6	209.1	2.34	0.31	
			159[a]			80.8[a]	207[a]	1.97[a]	0.29[a]	
o-Fe_3B	203.8	199.5	201.6	101.3	90.6	96.0	248.5	2.10	0.30	9.1
t-Fe_3B	175.1	173.1	174.1	102.2	94.2	98.2	248.0	1.77	0.26	12.0
Fe_2B	222.7	221.8	222.3	144.4	143.6	144.0	355.2	1.54	0.23	19.0
			228[b]			143[b]	355[b]	1.59[b]	0.24[b]	18.2[c]
FeB	287.8	284.6	286.2	148.5	130.9	139.7	360.5	2.05	0.29	12.5
			287[b]			138[b]	358[b]	2.08[b]	0.29[b]	
FeB_2	311.8	308.5	310.2	233.5	229.8	231.6	556.4	1.34	0.20	31.4
			311[b]			231[b]	556[b]	1.35[b]	0.20[b]	
FeB_4	283.4	266.9	275.2	194.9	181.4	188.1	459.6	1.46	0.22	24.4
			274[b]			187[b]	457[b]	1.46[b]	0.22[b]	
α-B	242.0	236.3	239.2	201.4	123.7	162.5	397.6	1.47	0.22	22.0

[a] Ref. [37].
[b] Ref. [5].
[c] Ref. [10].

anisotropy indexes. FeB, FeB_4 and two Fe_3B compounds exhibit certain degree of anisotropy. All of the six iron borides locate at the left bottom corner of the elastic anisotropy diagram [43].

The bulk and Young's moduli in three dimensions (3D) as a function of the crystallographic direction can be used as a more straightforward way to describe the elastic anisotropy. The 3D representation of Young's modulus for orthorhombic crystals in any direction is given by [14,44]:

$$\frac{1}{E} = s_{11}l_1^4 + s_{22}l_2^4 + s_{33}l_3^4 + (2s_{12} + s_{66})l_1^2l_2^2 + (2s_{13} + s_{55})l_1^2l_3^2 + (2s_{23} + s_{44})l_2^2l_3^2 \tag{31}$$

where l_1, l_2 and l_3 are the direction cosines. As an example, only the 3D representation and corresponding 2D projections of Young's moduli for FeB and Fe_2B compounds are presented in Fig. 3. For FeB which has the largest A^U value of 0.68, the anisotropy of Young's modulus is clearly illustrated in Fig. 3(a) and (b). The shear anisotropic indexes are 1.63, 0.91, 2.45 for (100), (010) and (001) planes, respectively. Correspondingly, the 2D projection of Young's modulus in xz plane is almost a regular ellipse, while in yz and xy planes the projections exhibit obvious anisotropy. However, for Fe_2B which has the smallest A^U value of 0.03, the anisotropy of Young's modulus is clearly much smaller than that of FeB.

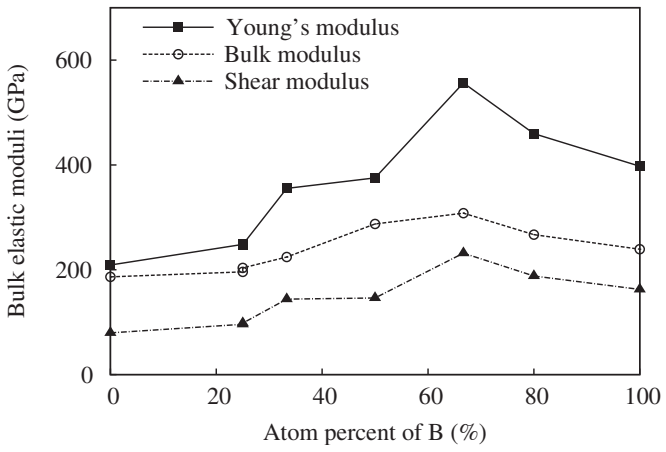

Fig. 2. Polycrystalline elastic moduli of Fe–B system.

The transverse and longitudinal acoustic velocities v_t and v_l can be obtained from the isothermal bulk and shear moduli [44]:

$$v_l = \sqrt{(B + 0.75G)/\rho}$$
$$v_t = \sqrt{G/\rho} \tag{32}$$

where ρ is the density. The corresponding average sound velocity v_m and Debye temperature are given by:

$$v_m = \left[\frac{1}{3}\left(\frac{1}{v_l^3} + \frac{2}{v_t^3}\right)\right]^{-\frac{1}{3}} \tag{33}$$

$$\Theta_D = \frac{h}{k_B}\left[\frac{3n}{4\pi}\left(\frac{N_A\rho}{M}\right)\right]^{\frac{1}{3}} v_m \tag{34}$$

where h, k_B and N_A are Planck, Boltzmann and Avogadro's constant, n is the number of atoms in the formula unit, M is the molecular weight. The results are presented in Table 5. It can be seen that the sound velocities and Debye temperatures increase with B atom contents from α-Fe to α-B.

3.3. Phonon and thermodynamic properties

The phonon dispersion curves and partial atomic phonon density of states (PhDOS) for FeB and Fe_2B are presented in Fig. 4(a) and (b). For the other four iron borides, only the total PhDOS are plotted in Fig. 4(c). There are no imaginary phonon modes for all of these compounds, indicating their dynamical stability.

The phonon spectrums for FeB and Fe_2B can be divided into three parts: (i) the low frequency modes (0–350 cm^{-1} for both FeB and Fe_2B) essentially contributed by Fe atoms together with slight contributions from B atoms. (ii) The mixed Fe–B modes in the medium frequency range (430–580 cm^{-1} for FeB and 350–460 cm^{-1} for Fe_2B). It is noted that for Fe_2B there is an obvious mixture of the Fe and B modes. (iii) The high frequency modes (620–780 cm^{-1} for FeB and 510–570 cm^{-1} for Fe_2B) mainly stem from B atoms. The phonon modes of FeB and Fe_2B are different from that of FeB_2, since for FeB_2 the mixed Fe and B modes emerge only in the low frequency range [4].

For all of the six compounds, the acoustic phonons are mainly contributed by Fe atoms, while the optical phonons mainly come from the vibrations of B atoms. This is in consistent with the fact that Fe atom is much heavier than B atom. The maximum frequency ω_m increases with B atom content. There are two phonon bandgaps in the whole frequency range for FeB, o-Fe_3B and t-Fe_3B. While for

Table 5
Anisotropic factors, sound velocities and Debye temperatures of Fe–B system.

Substances	A_1	A_2	A_3	A_B (%)	A_G (%)	A^U	v_l (m/s)	v_t (m/s)	v_m (m/s)	Θ_D (K)
α-Fe	1.61	1.61	1.61	0	2.64	0.27	5523	3140	3491	461
o-Fe_3B	1.72	1.53	2.12	1.07	5.58	0.61	6032	3572	3957	550
t-Fe_3B	1.17	1.17	2.34	0.57	4.07	0.44	5708	3594	3956	552
Fe_2B	1.07	1.07	1.23	0.20	0.28	0.03	6636	4382	4796	685
FeB	1.63	0.91	2.45	0.62	5.85	0.68	7509	4489	4968	740
FeB_2	1.28	0.79	0.93	0.53	0.80	0.09	9024	6243	6791	1046
FeB_4	1.55	0.61	1.07	3.00	3.58	0.43	9536	6411	7001	1080
α-B	1.05	1.05	1.00	1.19	23.9	3.17	12,075	8102	8849	1361

Fe_2B, FeB_2 and FeB_4, there are only one bandgap locates before the last phonon peak. For both o- and t-Fe_3B compounds, in the lower frequency range of $\omega < 350$ cm^{-1}, the phonon DOSs are similar to each other. However, in the higher frequency range, the vibrational frequency of o-Fe_3B shifts towards the higher frequency and ω_m of o-Fe_3B is larger than that of t-Fe_3B. This suggests the stronger bonding in o-Fe_3B. The phonon DOSs can be used to obtain the thermodynamic properties of these compounds.

The specific heat at constant pressure C_p, molar Gibbs free energy G_m with respect to the value at 298.15 K and molar entropy S_m of all the six Fe–B compounds are calculated from phonon method and Debye–Grüneisen model. In Debye model, the Grüneisen ratios from Slater, Dugdale–McDonald (DM) and Vaschenko–Zubarev (VZ) are utilized as mentioned in Section 2. For FeB and Fe_2B compounds, the related data obtained from CALPHAD method [9] based on the interstitial model are also presented. It should be noted that the CALPHAD results are composed of two parts: a major thermal contribution (hereafter denoted by C_{pt}, G_{mt} and S_{mt}) and a minor magnetic contribution, while the magnetic contributions are not considered in this work.

Thermodynamic properties C_p, G_m and S_m of FeB are presented in Fig. 5. Results derived from CALPHAD modeling [9] are represented as open triangles and open circles for the thermally contributed values and the total values, respectively. For the specific heat in Fig. 5(a), all the results obtained in this work agree well with the thermal part of CALPHAD data within the whole temperature range. Even for the total specific heat value, this work gives reasonable results except for the narrow temperature range around the Curie temperature of 600 K. Among the three Debye results, it is evident that the DM model Grüneisen ratio gives almost equivalent result with CALPHAD approach, while the Slater and VZ parameters give higher and lower results, respectively. The results obtained from phonon method are lower than other ones, which may be caused by the errors induced by limited supercell size, k-point sampling and the adopted parameters in phonon calculations. Meanwhile, the parameters in Debye model, for example the Debye temperature Θ_D and the Grüneisen ratio γ, usually play important roles in introducing the errors. Additionally, well converged energy–volume data points are required to derive accurate thermodynamic results, since scattered E–V points may cause larger errors especially at high temperatures.

For molar Gibbs energy G_m and molar entropy S_m in Fig. 5(b) and (c), all of the results are in good agreement with CALPHAD ones although G_m are a little smaller and S_m are a little larger, because the magnetic contributions to total Gibbs free energy and total entropy are small compared with vibrational contributions, which is not the case in determining specific heat. Since the CALPHAD results are usually optimized from room temperature (T_r) upward,

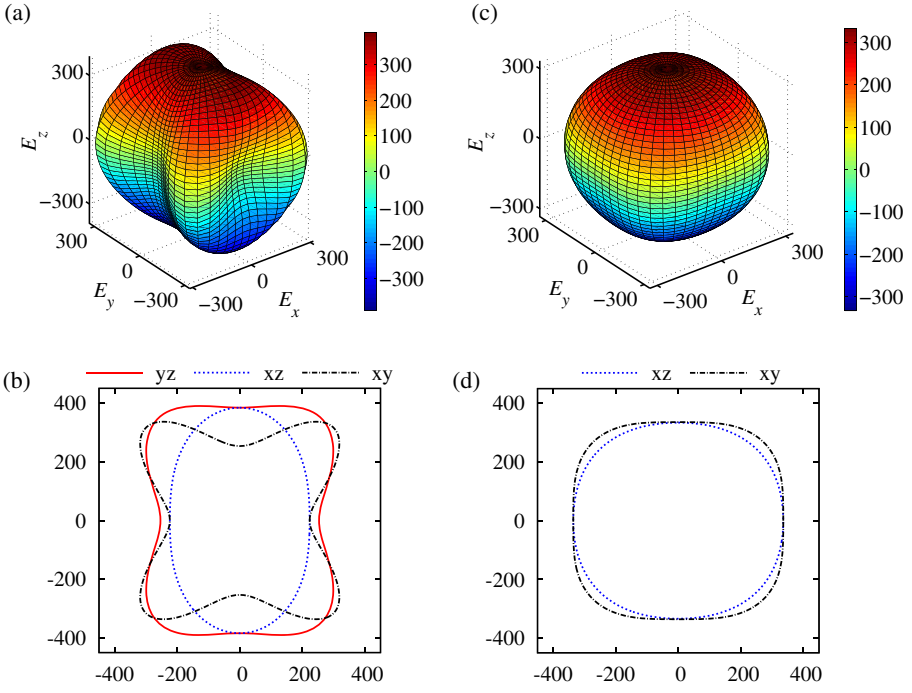

Fig. 3. The 3D representation and 2D projections of Young's moduli for (a)(b) FeB and (c)(d) Fe_2B compounds.

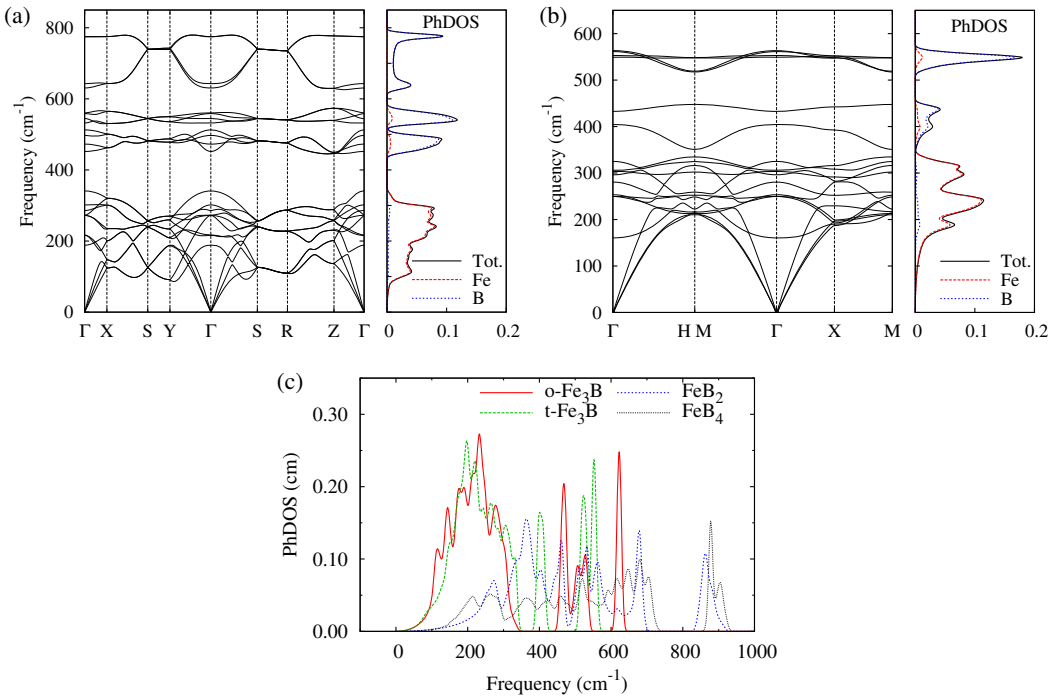

Fig. 4. Phonon properties of Fe–B compounds. (a)(b) Phonon dispersion and atom projected PhDOS for FeB and Fe_2B, respectively; (c) total PhDOS for FeB_2, FeB_4, *o*-Fe_3B and *t*-Fe_3B compounds.

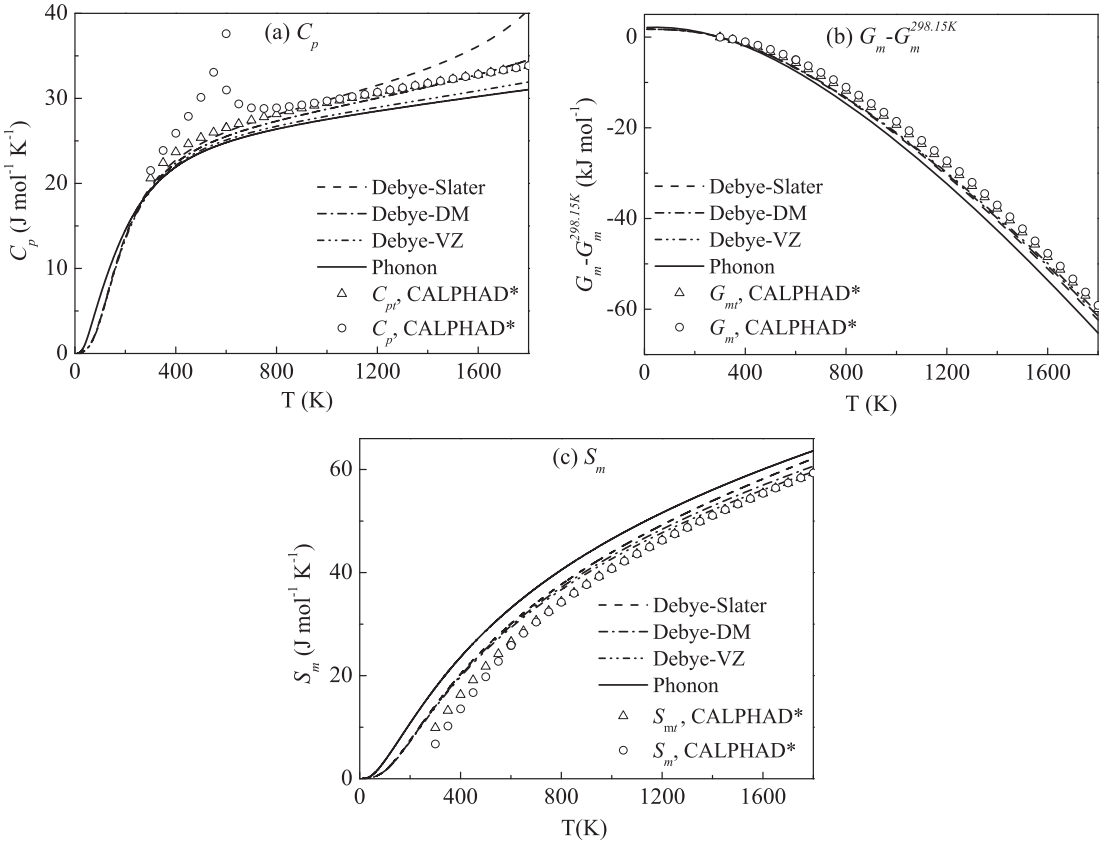

Fig. 5. The calculated thermodynamic properties of FeB: (a) Specific heat at constant pressure C_p (b) molar Gibbs free energy G_m with respect to 298.15 K and (c) molar entropy S_m. Thermal and total results derived from CALPHAD method (Ref. [9]) are denoted by open triangles and open circles, respectively.

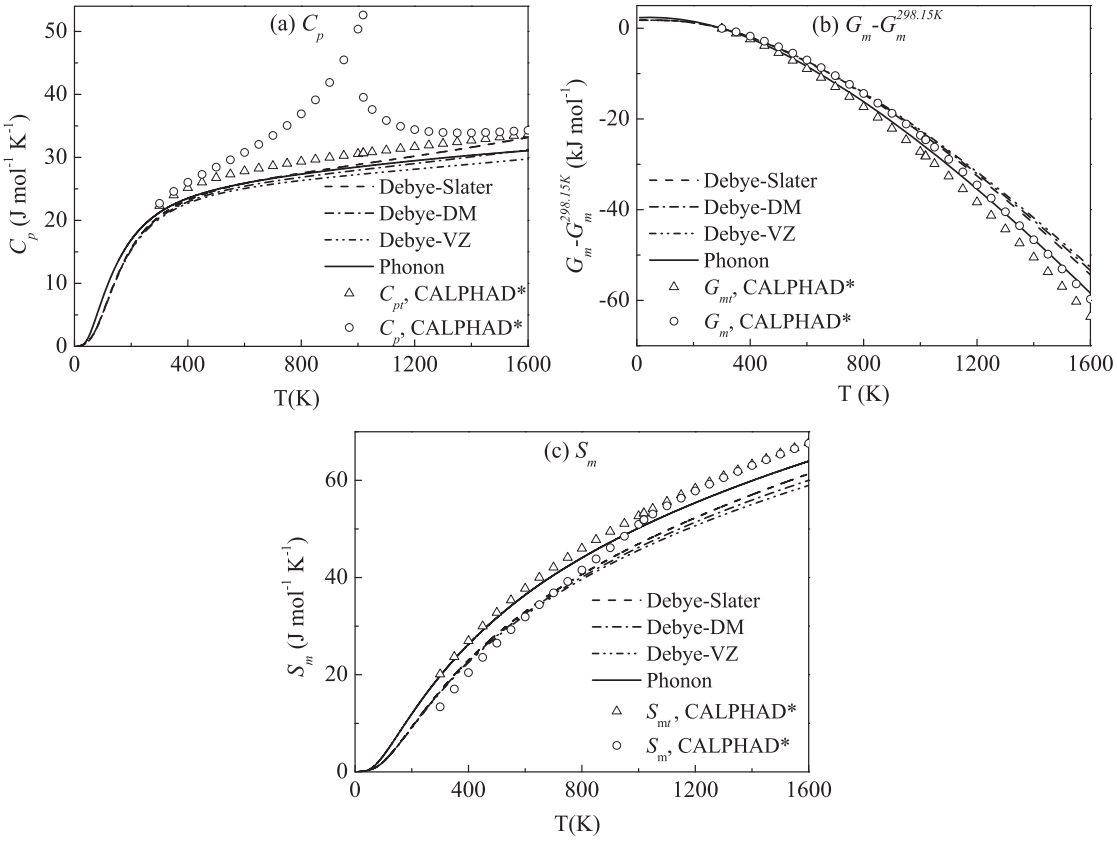

Fig. 6. The calculated thermodynamic properties of Fe_2B: (a) Specific heat at constant pressure C_p (b) molar Gibbs free energy G_m with respect to 298.15 K and (c) molar entropy S_m. Thermal and total results derived from CALPHAD method (Ref. [9]) are denoted by open triangles and open circles, respectively.

it should be mentioned that the molar entropy S_m are underestimated below T_r since it approaches to zero at 200 K, while this should in fact happen at 0 K. It can be concluded from the results that first-principle calculations together with Debye or phonon methods can provide more reasonable results for molar entropy of FeB.

The thermodynamic properties of Fe_2B are presented in Fig. 6. From Fig. 6(a), the phonon method and DM parameter in Debye model give quite similar results. The result from Slater ratio is the highest one and provides more accurate description of the specific heat. For Gibbs free energy in Fig. 6(b), the phonon method provides almost equivalent result with thermal part of CALPHAD one, when the temperature is lower than the Curie temperature of 1018 K. Even at temperature up to 1600 K near the melting point, the error is less than 6%. For the molar entropy, this work similarly gives quite good results especially for the phonon method, as shown in Fig. 6(c).

For the other four iron borides FeB_2, FeB_4, *o*-Fe_3B and *t*-Fe_3B, the C_p, G_m and S_m are calculated based on both Debye and phonon models. However, since the results vary only a little from different Debye models and the lattice phonons may be not stable for metastable phases, only the results obtained from Debye model based on DM parameters are presented in Fig. 7.

From Fig. 7(a), the specific heats of *o*- and *t*-Fe_3B compounds are larger than those of FeB_2 and FeB_4 at temperatures lower than 1200 K. For both two Fe_3B compounds, *t*-Fe_3B has larger specific heat than *o*-Fe_3B in the whole temperature range. From Fig. 7(b) and (c), the absolute values of G_m for both *o*- and *t*-Fe_3B compounds are very close to each other and larger than those of FeB_2 and FeB_4, which is the same case for S_m. The insets of Fig. 7(b) and (c) indicate that the differences of both G_m and S_m for *o*- and *t*-Fe_3B compounds are rather small. Even at temperatures larger than 1500 K, the differences of G_m are less than 0.2 kJ mol^{-1} and for S_m they are smaller than 0.6 J mol^{-1} K^{-1}. Although there are no available reference thermodynamic data for these four compounds, it is expected that this work has also provided reasonable thermodynamic data. According to the above discussions, it can be concluded that the thermodynamic properties can be accurately predicted by first-principle calculations together with phonon or Debye–Grüneisen model even in high temperatures.

The phase stability and phase transition of *o*- and *t*-Fe_3B are of considerable importance, it has been shown that *o*-Fe_3B is more stable than *t*-Fe_3B. It is well known that the energy of a structure will vary with applied external pressure. The phase transition pressure of two compounds can be derived from the enthalpy difference based on the EOS data. By using the thermodynamic model described in Section 2, the enthalpy difference of *t*-Fe_3B to *o*-Fe_3B versus applied external pressure at 0 K is calculated and presented in Fig. 8. The phase transition pressure is found to be 8.3 GPa.

4. Conclusions

This work presents the first-principle calculated structural, elastic, phonon and thermodynamic properties for FeB, Fe_2B, orthorhombic and tetrahedral Fe_3B, FeB_2 and FeB_4 iron borides. The results indicate that the equilibrium structural properties can be accurately predicted by first-principle calculations together with EOS fitting to the energy–volume curves.

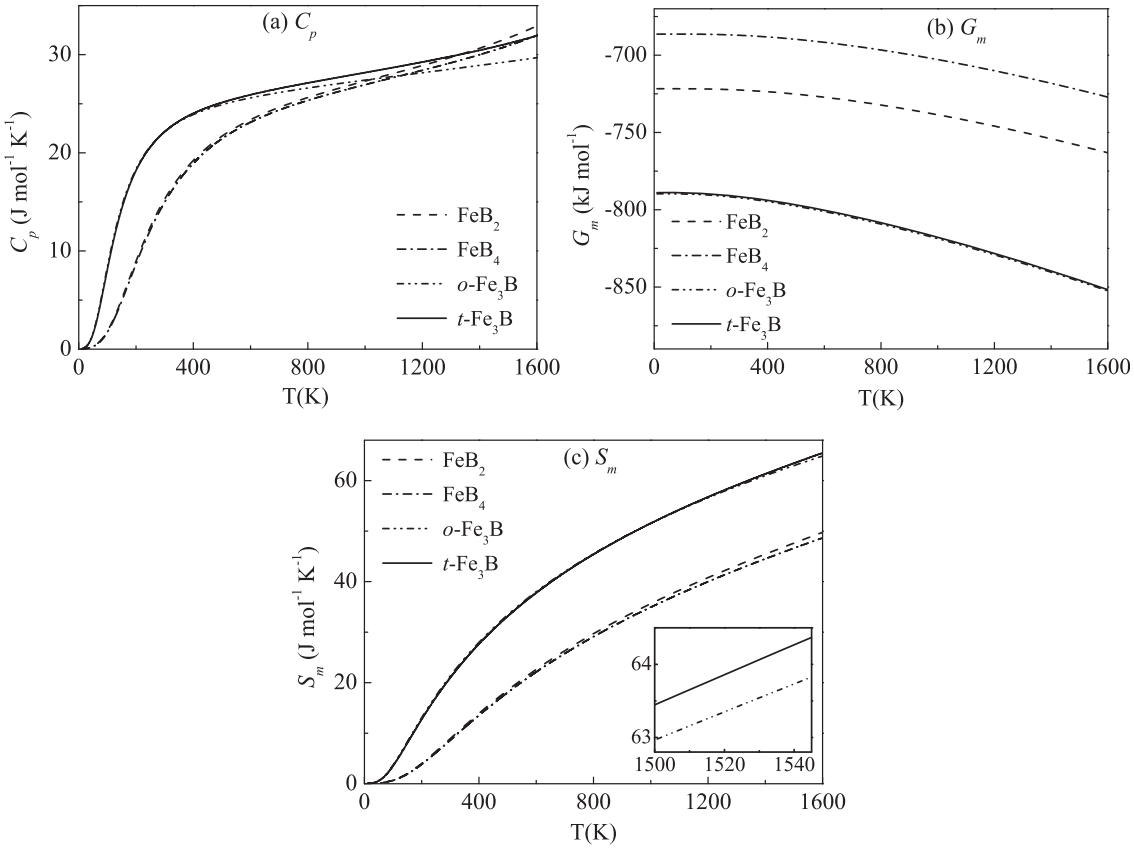

Fig. 7. The calculated thermodynamic properties of FeB_2, FeB_4, *o*-Fe_3B and *t*-Fe_3B: (a) Specific heat at constant pressure C_p (b) molar Gibbs free energy G_m and (c) molar entropy S_m.

The single crystalline elastic constants and polycrystalline elastic moduli of Fe–B compounds are found to be large especially for FeB_2 and FeB_4, since the maximum elastic constant exceeds 700 GPa and the polycrystalline bulk moduli of all the six iron borides are larger than that of pure Fe. All of the six Fe–B compounds are mechanically stable. The ratios of *B*/*G* and Poisson's ratios indicate that FeB, *o*-Fe_3B and *t*-Fe_3B can be characterized as ductile, while Fe_2B, FeB_2 and FeB_4 should be classified as brittle. The Vickers hardness of FeB_2 is 31.4 GPa, suggesting that this material may be very hard. FeB, FeB_4, *o*-Fe_3B and *t*-Fe_3B compounds exhibit strong anisotropy concluded from the anisotropic indexes, three dimensional representation and two dimensional projections of Young's modulus, while Fe_2B and FeB_2 are almost isotropic. The average sound velocities and Debye temperatures of these compounds increase with B atom contents.

The phonon dispersion spectrums and phonon density of states indicate that these iron borides are dynamically stable. Thermodynamic properties of Fe–B compounds can be accurately predicted by first-principle calculations together with quasi-harmonic approximation, especially for the molar Gibbs energy and molar entropy. The *o*-Fe_3B compound is found to be more stable than *t*-Fe_3B based on the enthalpy difference, and the phase transition pressure is estimated to be 8.3 GPa.

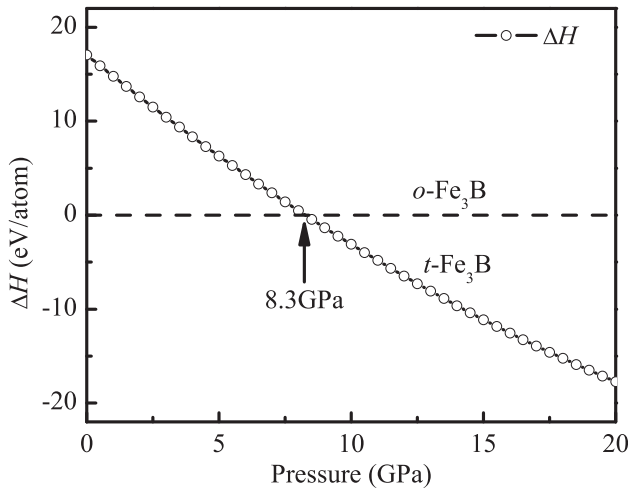

Fig. 8. Enthalpy difference of *t*-Fe_3B to *o*-Fe_3B as a function of applied external pressure.

Acknowledgments

This work was financially supported by the National Natural Science Foundation of China (Nos. 51271150 and 51101123), and the Fundamental Research Fund of Northwestern Polytechnical University (JC20120245). The authors are very grateful to the helpful discussions with Dr. Zhen-Yu Hong and Jian Chang.

References

[1] Ching WY, Xu Y-N, Harmon BN, Ye J, Leung TC. Phys Rev B 1990;42:4460–70.
[2] Bratkovsky AM, Rashkeev SN, Wendin G. Phys Rev B 1993;48:6260–70.
[3] Kong Y, Li F. Phys Rev B 1997;56:3153–8.
[4] Kolmogorov AN, Shah S, Margine ER, Bialon AF, Hammerschmidt T, Drautz R. Phys Rev Lett 2010;105:217003.
[5] Bialon AF, Hammerschmidt T, Drautz R, Shah S, Margine ER, Kolmogorov AN. Appl Phys Lett 2011;98:081901.
[6] Tian H, Zhang C, Zhao J, Dong C, Wen B, Wang Q. Physica B 2012;407:250–7.

[7] Sánchez FH, Fernández van Raap MB, Budnick JI. Phys Rev B 1992;46:13881–8.
[8] Battezzati L, Antonione C, Baricco M. J Alloy Compd 1997;247:164–71.
[9] Van Rompaey T, Hari Kumar KC, Wollants P. J Alloy Compd 2002;334:173–81.
[10] Xiao B, Feng J, Zhou CT, Xing JD, Xie XJ, Cheng YH, et al. Physica B 2010;405:1274–8.
[11] Wang Y, Liu Z-K, Chen L-Q. Acta Mater 2004;52:2665–71.
[12] Shang S-L, Wang Y, Kim D, Liu Z-K. Comp Mater Sci 2010;47:1040–8.
[13] Arróyave R, Liu Z-K. Phys Rev B 2006;74:174118.
[14] Panda KB, Ravi Chandran KS. Acta Mater 2006;54:1641–57.
[15] Wu Z-J, Zhao E-J, Xiang H-P, Hao X-F, Liu X-J, Meng J. Phys Rev B 2007;76:054115.
[16] Blanco MA, Francisco E, Luaña V. Comput Phys Commun 2004;158:57–72.
[17] Otero-de-la-Roza A, Abbasi-Pérez D, Luaña V. Comput Phys Commun 2011;182:2232–48.
[18] Otero-de-la-Roza A, Luaña V. Comput Phys Commun 2011;182:1708–20.
[19] Otero-de-la-Roza A, Luaña V. Phys Rev B 2011;84:024109.
[20] Perdew JP, Chevary JA, Vosko SH, Jackson KA, Pederson MR, Singh DJ, et al. Phys Rev B 1992;46:6671–87.
[21] Perdew JP, Burke K, Ernzerhof M. Phys Rev Lett 1996;77:3865–8.
[22] Blöchl PE. Phys Rev B 1994;50:17953–79.
[23] Kresse G, Hafner J. Phys Rev B 1993;47:558–61.
[24] Kresse G, Furthmüller J. Phys Rev B 1996;54:11169–86.
[25] Monkhorst HJ, Pack JD. Phys Rev B 1976;13:5188–92.
[26] Methfessel M, Paxton AT. Phys Rev B 1989;40:3616–21.
[27] Blöchl PE, Jepsen O, Andersen OK. Phys Rev B 1994;49:16223–33.
[28] Togo A, Oba F, Tanaka I. Phys Rev B 2008;78:134106.
[29] Togo A http://sourceforge.net/projects/phonopy/.
[30] Gonze X, Lee C. Phys Rev B 1997;55:10355–68.
[31] Jarlborg T, Moroni EG, Grimvall G. Phys Rev B 1997;55:1288–91.
[32] Villars P, Cenzual K. Pearson's crystal data – crystal structure database for inorganic compounds (on CD-ROM). Release 2011/12. Materials Park, Ohio, USA: ASM International; 2011.
[33] Kittel C. Introduction to solid state physics. 7th ed. John Wiley & Sons Inc.; 1996.
[34] Kong Y, Xiong W, Guo H, Sun W, Du Y, Zhou Y. CALPHAD 2010;34:245–51.
[35] Liang YF, Shang SL, Wang J, Wang Y, Ye F, Lin JP, et al. Intermetallics 2011;19:1374–84.
[36] Shang S, Wang Y, Arroyave R, Liu Z-K. Phys Rev B 2007;75:092101.
[37] Hill R. Proc Phys Soc Lond Sect A 1952;65:349–54.
[38] Shang SL, Saengdeejing A, Mei ZG, Kim DE, Zhang H, Ganeshan S, et al. Comp Mater Sci 2010;48:813–26.
[39] Gao F, He J, Wu E, Liu S, Yu D, Li D, et al. Phys Rev Lett 2003;91:015502.
[40] Šimůnek A, Vackář J. Phys Rev Lett 2006;96:085501.
[41] Li K, Wang X, Zhang F, Xue D. Phys Rev Lett 2008;100:235504.
[42] Chen X-Q, Niu H, Li D, Li Y. Intermetallics 2011;19:1275–81.
[43] Ranganathan S, Ostoja-Starzewski M. Phys Rev Lett 2008;101:055504.
[44] Feng J, Xiao B, Zhou R, Pan W, Clarke DR. Acta Mater 2012;60:3380–92.